Applied Biochemistry and Biotechnology (2024) 196:3553–3575
https://doi.org/10.1007/s12010-023-04697-2

ORIGINAL ARTICLE

Identification, Characterization, and Computer-Aided Rational Design of a Novel Thermophilic Esterase from *Geobacillus subterraneus*, and Application in the Synthesis of Cinnamyl Acetate

Jin Zhang[1] · Lin Lin[2,3] · Wei Wei[1] · Dongzhi Wei[1]

Accepted: 16 August 2023 / Published online: 15 September 2023

Abstract
Investigation of a novel thermophilic esterase gene from *Geobacillus subterraneus* DSMZ 13552 indicated a high amino acid sequence similarity of 25.9% to a reported esterase from *Geobacillus* sp. A strategy that integrated computer-aided rational design tools was developed to select mutation sites. Six mutants were selected from four criteria based on the simulated saturation mutation (including 19 amino acid residues) results. Of these, the mutants Q78Y and G119A were found to retain 87% and 27% activity after incubation at 70 °C for 20 min, compared with the 19% activity for the wild type. Subsequently, a double-point mutant (Q78Y/G119A) was obtained and identified with optimal temperature increase from 65 to 70 °C and a 41.51% decrease in K_m. The obtained $T_{1/2}$ values of 42.2 min (70 °C) and 16.9 min (75 °C) for Q78Y/G119A showed increases of 340% and 412% compared with that in the wild type. Q78Y/G119A was then employed as a biocatalyst to synthesize cinnamyl acetate, for which the conversion rate reached 99.40% with 0.3 M cinnamyl alcohol at 60 °C. The results validated the enhanced enzymatic properties of the mutant and indicated better prospects for industrial application as compared to that in the wild type. This study reported a method by which an enzyme could evolve to achieve enhanced thermostability, thereby increasing its potential for industrial applications, which could also be expanded to other esterases.

Keywords Thermophilic esterase · Rational design · Thermal stability · ADAP strategy · Cinnamyl acetate

Introduction

Energy evolution and climate variation have remolded the world, which have forced humans to consider sustainable development trajectories [1]. Consequently, biocatalysts are now extensively employed in the industry. Biological catalysis is achieved under mild, ecologically friendly, and energy-saving conditions as compared to chemical catalysis. Lipolytic enzymes, such as lipases and esterases, are important enzyme families that are employed in the production of beverages, detergents, fine chemicals, cosmetics, and

Extended author information available on the last page of the article

pharmaceuticals [2]. Unlike lipases (EC3.1.1.3), esterases (EC 3.1.1.1) use tributyrin as a standard substrate, which hydrolyzes acylglycerols with an acyl chain length of less than 10 carbon atoms [3, 4]. Esterases belong to the α/β hydrolases superfamily in which a catalytic triad plays a crucial role in enzymatic activity. The different origins of esterases, which are widespread across plants, animals, and microbes, endow the enzymes with different attributes [5]. Thermophilic esterases, which are frequently isolated from thermophilic microorganisms [6], have significant advantages over mesophilic esterases in terms of thermal stability and resistance to denaturants and organic solvents and have thus been the focus of research in the field of biocatalysis in recent years [7]. However, the thermostability of thermophilic esterases that have been isolated from thermophiles does not necessarily satisfy the requirements for industrial application.

Site-directed evolution has developed rapidly over the past 30 years, during which more sophisticated methods have been integrated and applied to improve the characteristics of various enzymes [8]. The time-consuming and inefficient reliance on random mutations has therefore been abandoned by an increasing number of researchers. Multifarious methods are employed to enhance thermal stability, organic solvent tolerance, and enzymatic activity, all of which are crucial properties of biocatalysts [9, 10]. Among the extensively applied construction methods, site-directed mutations based on hotspots and rational design are the two most effective schemes. Hotspots can be divided into two categories: 3D structure-based hotspots and sequence-based hotspots [11]. Mutations based on hotspots disturb the 3D structure of the enzyme minimally and do not influence the global protein fold. Furthermore, screening for potential mutation sites at the amino acid level can minimize the associated library size while increasing the positive rates and efficiencies. Han et al. [12] employed the principle of hotspots by applying multiple sequence alignment (MSA) to enhance the stability of xylanase. MSA exhibited the most frequent amino acid that appeared at the specific position among homologous genes. Wang et al. [13] enhanced the thermostability of amylase using combinational coevolving-site saturation mutagenesis (CCSM), which was based on a subfamily evolution strategy. The protocol linked the hotspots of the subfamily regions to site saturation mutagenesis and enhanced the thermostability of the enzyme by 8 °C. In contrast to hotspots, site-directed mutation that is based on rational design is a more purposeful approach that is extremely accurate and result-oriented [14, 15]. However, exploring the influence of each amino acid during the folding process presents a significant challenge when applied to predict optimized mutations [16]. Fortunately, the recent accumulation of high-resolution crystal structures of various proteins, coupled with surging comprehension of the structural determinants of their properties, has provided a rationale by which the rational design of enzymes can be obtained without relying on random mutagenesis to improve enzymatic properties [17]. In 2020, Alessandro et al. employed rational design to investigate the role of the brain protein, TRIP8b, in restricting the cAMP response to HCN channels in neurons, and they found that a mutation in the loop connecting CNBD significantly reduced its binding to TRIP8b, indicating the crucial role of the loop in its affinity [18]. Computer-dependent rational design has also been employed in medicine to enhance curative effects, such as DNA binding affinity [19]. In brief, rational design can accelerate enzyme engineering with more powerful, effective, and accurate productivity.

Cinnamyl acetate, a natural essential oil, is widely used in beverages, personal care products, and cosmetics [20]. Chemical synthesis and natural extraction are generally employed for cinnamyl acetate production, leading to environmental damage [21]. Biocatalysis is the predominant application used in preparing enzymes with high stoichiometric efficiency [22]. However, the low conversion rate of enzyme-catalyzed cinnamyl acetate

synthesis is a major challenge hindering its large-scale application. Geng et al. [23] applied Novozyme 435 to synthesize cinnamyl acetate, with a 90.06% conversion rate obtained after conditions of optimization. The porcine pancreatic lipase has also been used to synthesize cinnamyl acetate; however, a conversion rate of only 62.56% has been obtained using this method [24]. Employing whole-cell catalysts to produce cinnamyl acetate would significantly reduce the cost of using biocatalysts in cinnamyl acetate production, while also decreasing the environmental destruction. However, a conversion rate of only 94.10% for cinnamyl acetate has been obtained using the whole-cell esterase catalyst from *Acinetobacter hemolyticus* [25]. The conversion rate is the most predominant index in biocatalysis, and a higher conversion rate for enzyme-catalyzed reactions is a common goal of biochemists.

In this study, a novel thermophilic esterase gene from the strain *Geobacillus subterraneus* DSMZ 13552 was expressed in *Escherichia coli*, and enzyme characteristics were described, including activity/stability, optimum pH, optimum temperature, and substrate specificity. To enhance the thermal stability, the rational design tools AutoDock, Discovery Studio, and PoPMuSiC (ADAP) were applied to design and select several mutants and analyze the enzymatic properties of the mutants. A double-point mutant was used for transesterification to synthesize the cinnamyl acetate using vinyl acetate and cinnamyl alcohol as substrates, and a conversion rate of 99.40% was achieved. In conclusion, mutants with improved thermal stability can be obtained using the ADAP strategy. Finally, the obtained mutant was used in the synthesis of cinnamyl acetate, for which it exhibited great enzymatic properties and can thus be considered for industrial application.

Materials and Methods

Strains and Plasmids

The strains and plasmids used in this study are listed in Table S1. The strain DSMZ 13552 (*G. subterraneus* DSMZ 13552) was obtained from Deutsche Sammlung von Mikroorganismen and Zellkulturen GmbH (DSMZ). *E. coli* DH5α (Novagen) was used for gene cloning, and *E. coli* BL21 (DE3) and plasmid pET-28a (+) (Novagen) were used to construct the heterologous esterase expression strains.

Chemicals and Culture Conditions

LA Taq polymerase, T4 DNA ligase, DNA markers, and restriction endonucleases (*Bam*H I and *Eco*R I) were purchased from TaKaRa Bio Inc. (Shiga, Japan). Protein markers were purchased from MBI Fermentas (Vilnius, Lithuania). Isopropyl-β-D-thiogalactopyranoside (IPTG) and kanamycin were purchased from Amresco (Shanghai Genebase Co., Ltd., China). The DNA Mini Kit and Plasmid Mini Preparation Kit were purchased from Axygen Biosciences (Union City, CA, USA). The substrates pNP-acetate (C2), pNP-butyrate (C4), pNP-hexanoate (C6), pNP-caprylate (C8), pNP-decanoate (C10), pNP-laurate (C12), pNP-myristate (C14), and pNP-palmitate (C16) were purchased from Sigma-Aldrich (St. Louis, MO, USA). All other chemicals were obtained commercially and were of reagent grade. Tributyrin medium (yeast extract 0.3%, tryptone 1.0%, NaCl 1.0%, agar 1.8%, and 2% tributyrin emulsion (v/v)) was used for verification of enzyme activity. Medium 1

(peptone 0.5%, meat extract 0.3%, and $MnSO_4$ (0.05 mM), pH 7.0) was used for *G. subterraneus* cultivation at 60 °C.

All experiments were performed in triplicate, and the results were presented as the average of the obtained values with standard deviation.

Cultivation and Measurement of *G.* subterraneus DSMZ 13552

The strain *G. subterraneus* DSMZ 13552 was fermented at 60 °C to determine its growth rate and esterase activity. Every 2 or 4 h, 1 mL of fermentation broth was transferred to the Eppendorf tube (3 tubes at a time), and the cell concentration (OD_{600}) and enzyme activity of the supernatant were measured.

Sequence Analyses and Homology Modeling

BLASTN and BLASTP (NCBI) were employed to analyze the nucleotide and predicted amino acid sequences by revealing sequence similarities and evolutionary distance. Sequences were aligned using ClustalX2 [26] allowing further exploration of the detailed similarities, and ESPript 3.0 (https://espript.ibcp.fr/ESPript/ESPript/) [27] was applied to render the results. The ExPASy proteomics web server (http://web.expasy.org/compute_pi/) [28] was used to calculate the molecular weight (Mw) and isoelectric point (pI) of the enzymes, and SOPMA (https://npsa-pbil.ibcp.fr/cgi-bin/npsa_automat.pl?page=npsa_sopma.html) was employed to ascertain the proportion of secondary structures. The AlphaFold Protein Structure Database (https://alphafold.ebi.ac.uk) [29, 30] was used to predict the three-dimensional structures of the enzymes. PyMOL was applied to visualize the 3D structure of the wild-type (WT) enzyme and its mutants, with amino acid residues and secondary structures displayed using different colors and modes. The final models were validated via PROCHECK (http://services.mbi.ucla.edu/PROCHECK) and Verify 3D [31–33].

Gene Cloning and Expression of gsu768 in *E.* coli

The genome of *G. subterraneus* DSMZ 13552 was collected using a bacterial genome extraction kit from Generay Biotechnology, China. Primers (U:5′-cagcaaatgggtcgcggatccATGGTGATCATTGAACAGGAACAG-3′; D:5′-ttgtcgacggagctcgaattcTTACACATGCTCGCGAAACCA-3′; F:5′-atgggtcgcggatccgaattcATGGTGATCATTGAACAGGAACAG-3′; R:5′-ttgtcgacggagctcgaattcTTACACATGCTCGCGAAACCA-3′) were designed using the primer design software CE Design (v1.04) and used for gsu768 amplification. U and D were used to amplify the original gsu768 with double-restriction endonuclease cutting sites (*Bam*H I and *Eco*R I), and F and R to amplify the mutated gsu768. PCR was then used to further amplify gsu768 using the collected genome as a template, and the product was verified and purified by agarose gel electrophoresis. At the same time, *E. coli* (DH5α) harboring pET-28a (+) was cultivated to extract vector pET-28a (+). Subsequently, gsu768 was linked to the vector digesting with *Bam*H I and *Eco*R I using the T4 ligase to construct BL21-pET-28a-gsu768, and the mutant gsu768 linked to the vector digesting with *Eco*R I via one-step cloning (Vazyme, China) to obtain strains that harbored mutants. Finally, the linkage products were transformed into *E. coli* BL21 (DE3) separately to construct heterologous expression strains. To obtain recombinant esterase Gsu768 from *E. coli* BL21 (DE3), *E. coli* BL21 (DE3) was incubated with recombinant plasmids in LB medium containing kanamycin (50 μg/mL) at 37 °C. After the optical density at 600 nm (OD_{600}) reached 0.6, IPTG (24 μg/mL terminal concentration)

was added for protein induction, and the cells were cultivated at 20 °C for another 20 h. Cell pellets were disrupted by sonication (work 3 s, stop 5 s, 200 W) on ice for 15 min, and supernatant including soluble esterase Gsu768 was obtained (8000×g for 10 min, 4 °C).

Selection of Mutation Sites via the ADAP Strategy

The computer-aided rational design strategy ADAP (Autodock, Discovery Studio, and PoPMuSiC) was applied to select the mutation sites (Fig. 1a). AutoDock 4.2.6 [34] which has been used for molecular docking between Gsu768 and C6 was employed to identify the substrate-binding pocket. Briefly, the hydrogen atoms and the Gasteiger charges on Gsu768 and C6 were saved in the.pdbqt format, and the grid box dimensions and center point coordinates were set to 50 Å × 60 Å × 50 Å and 88.259, 46.593, and 16.941, respectively. The Lamarckian genetic algorithm was then applied for molecular docking with the number of docking poses extended from 10 to 100. The highest binding affinity and corresponding interaction conformations were verified and visualized using Discovery Studio software. The Predict Stable Mutations module in Discovery Studio 3.5 was used to predict mutations in the key residues located in the pocket. Subsequently, changes in the protein thermodynamic stability of single-site mutation were predicted using PoPMuSiC (https://soft.dezyme.com/) [35]. Mutations were selected under four criteria: (1) mutants should have key residues in the substrate-binding pocket and with mutation energy < 0; (2) mutants should show ΔΔG < 0 in PoPMuSiC; (3) mutations should have ΔTm > 0 in HoTMuSiC; (4) mutations should show thermal stability of + in SNPMuSiC. Mutations that met all four criteria were used in the subsequent experiments.

Site-Directed Mutagenesis

Site-directed gsu768 mutagenesis was performed using the quick-change site-directed mutagenesis method (Stratagene, CA, USA), with the recombinant plasmid pET-28a-gsu768 as the template. PCR products were incubated with *Dpn* I at 37 °C for 1.5 h to digest the original plasmid and then transformed into *E. coli* DH5α. Verified plasmids were then transformed into *E. coli* BL21 (DE3) for expression analysis. The mutant structures were predicted using the constructed WT homology model as a template. All generated models were evaluated and verified by the Ramachandran plot.

Enzymatic Property Analysis

Enzymatic activity was determined by spectrophotometry after 5 min of reaction at various temperatures (55 °C, 60 °C, 65 °C, 70 °C, 75 °C, and 80 °C), and the amount of p-nitrophenol formed by the hydrolysis of pNP-hexanoate was measured at 405 nm. The optimal temperature of the enzyme was assayed over a range of temperatures from 55 to 80 °C. The optimum pH for the enzyme activity was studied over incubation in a range of pH values (7.0–10.0) for 5 min at the optimal temperature. One unit of enzyme activity (U) was defined as the amount of enzyme required to release 1 μM p-nitrophenol per min. Thermal stability was determined by measuring the residual enzyme activity after the enzyme was exposed separately to different temperatures over different periods (5 or 15 min). The half-life of esterase ($T_{1/2}$) was plotted by incubating the enzyme at various temperatures over different time intervals. The enzyme activity was considered 100% at the start of the

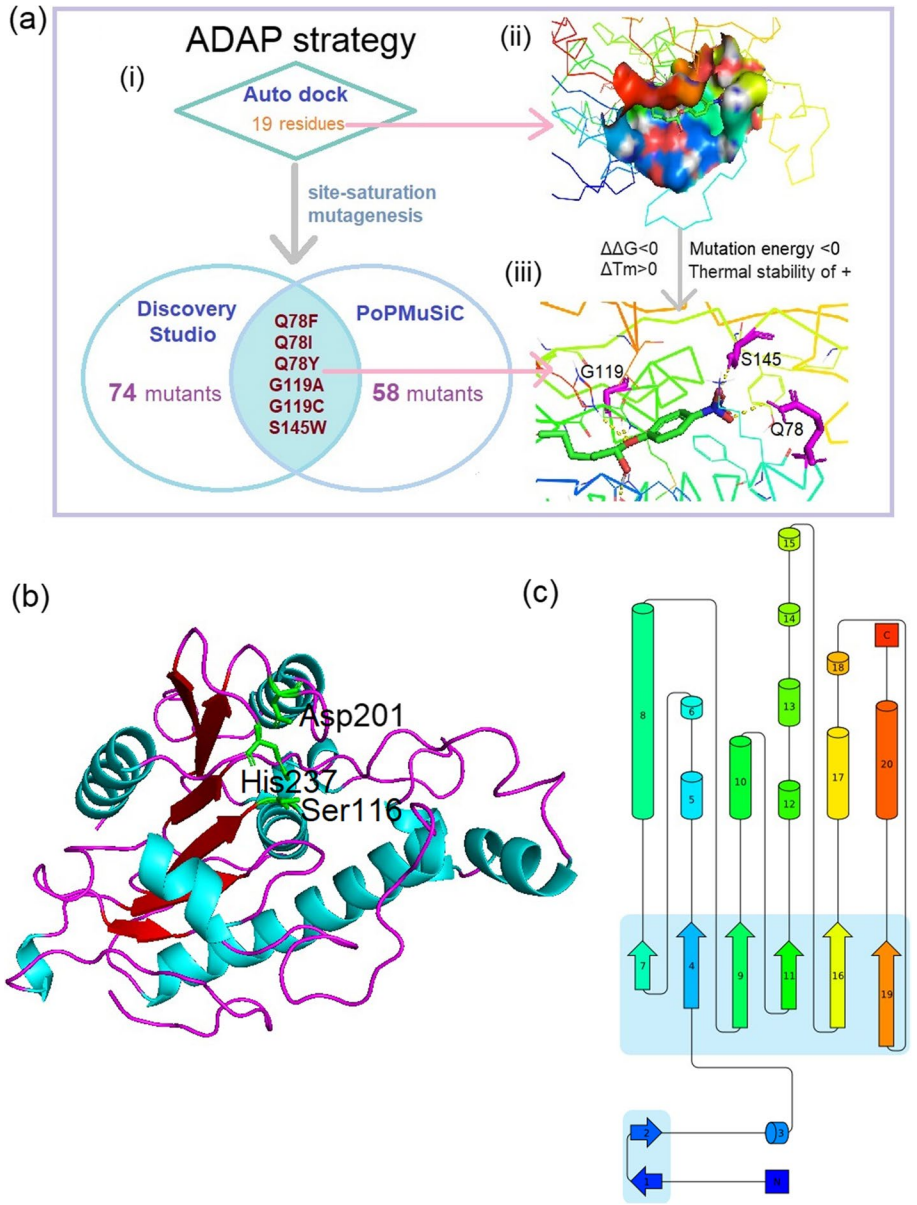

Fig. 1 Flowchart for predicting mutants with excellent thermal stability by ADAP strategy and structure of Gsu768. **a** ADAP strategy. (i) ADAP strategy flowchart. (ii) Schematic diagram of substrate combination pocket obtained after docking. (iii) The position of mutant residues in three-dimensional space. **b** The three-dimensional structure. The three-dimensional structure of Gsu768 was predicted by the AlphaFold Protein Structure Database. The catalytic triad: Ser116, Asp201, and His237 residues were shown with the green sticks. **c** Topology diagram. The distribution of secondary structure elements of α/β structure

experiment, and the residual esterase activity after incubation for different time intervals was measured and analyzed. To explore the effect of different concentrations of metal ions on enzyme activity, the activities of Gsu768 and its mutants were analyzed in the presence of different metal ions ($MnCl_2$, $CoCl_2$, $CaCl_2$, $CuCl_2$ $ZnCl_2$, $MgCl_2$, and $FeSO_4$) at final concentrations of 1, 5, and 10 mM by incubating in 50 mM Tris–HCl (pH 9.0) at the optimal temperature for 30 min. The influence of chemical reagents (Tween 20, Tween 80, sodium dodecyl sulfonate (SDS), and Triton X-100) was analyzed by incubation in 50 mM Tris–HCl (pH 9.0) at the optimal temperature for 30 min at final concentrations of 1% and 10% (v/v). The organic solvent (ethyl acetate, acetone, n-hexane, acetonitrile, isooctane, 1,4-dioxane, and trichloromethane) tolerance was analyzed by incubating the enzyme with organic solvents at final concentrations of 50% and 90% (v/v). The activity of the non-incubated enzyme was determined as 100% activity.

Purification and Determination of Kinetic Parameters

A Ni–NTA Superflow Column (1 mL, Qiagen, Hilden, Germany) was used to collect the target protein. The protein that bound to the column was eluted with a linear gradient of imidazole (from NPI 20 to NPI 250). Sodium dodecyl sulfate–polyacrylamide gel electrophoresis (SDS-PAGE) was used to evaluate crude and purified proteins. The Michaelis–Menten constant (Km) and the maximum velocity for the reaction (OD_{405}) of Gsu768 and its mutants were determined using serial concentrations of pNP-esters (0.03–0.30 mM) as substrates and assayed using the p-nitrophenol method (pH 9.0 and 65 or 70 °C). Kinetic data were calculated using the Lineweaver–Burk plot and the Michaelis–Menten equation.

Synthesis of Cinnamyl Acetate

Cinnamyl acetate was synthesized via transesterification using a whole-cell catalyst. Cells containing esterase Gsu768 were lyophilized by vacuum freezing, and the dried whole cells were used as a catalyst. The reaction was conducted in a 25 mL round bottom glass reactor that was partially immersed in a thermostatic water bath at the desired temperature. Organic solvents affect not only the solubility of hydrophobic substrates but also their enzymatic activity toward the substrates. Solvents n-hexane, acetonitrile, acetone, isooctane, trichloromethane, ethyl acetate, and 1,4-dioxane were tested and various factors affecting the conversion rate of the reaction investigated: (1) the molar ratio of cinnamyl alcohol and vinyl acetate was modified to 1:1, 1:2, 1:4, 1:6, 1:8, 1:10, and 1:15, and the concentration of cinnamyl alcohol was maintained at 0.3 M. (2) The whole-cell catalyst dosages ranged from 0.010 to 0.030 g/mL per reaction. (3) The effect of reaction temperature was verified at 30 °C, 40 °C, 50 °C, 55 °C, 60 °C, 65 °C, and 70 °C, with other conditions consistent with the above data. (4) The reaction time was set to 4, 8, 12, 20, 24, 28, 32, and 36 h to explore the influence of time. The product was directly detected by thin-layer chromatography (TLC) with hexane:ethyl acetate (85:15, v/v) as the mobile phase [36] and a 7820A gas chromatograph (GC) (Agilent Technologies, USA) equipped with a flame ionization detector (FID) was used to calculate the conversion rate [37]. The stationary phase was an HP-5 capillary column (30 m × 250 μm × 0.25 μm) and the mobile phase was nitrogen [25]. A parallel reaction without the catalyst was used as the control, and the conversion rate (%) was determined by the conversion of cinnamyl alcohol to cinnamyl acetate.

Results and Discussion

Fermentation of Wild Strain

The OD_{600} with respect to *G. subterraneus* DSMZ 13552 growth was determined following cultivation in medium 1 (at 60 °C). The strain grew slowly during the first 2 h, with exponential growth occurring between 2 and 12 h, and the cell concentration (OD_{600}) reaching 1.4 at 12th h. The highest enzymatic activity was observed at 18th h (Fig. S1a). To visualize the activity of esterase as compared to that in the WT strain, tributyrin was employed to produce a visible transparent zone, in accordance with the esterase activity (Fig. S1b).

Sequence and Structure Analysis of Gsu768

A 768 bp DNA fragment (denoted gsu768) from *G. subterraneus* DSMZ 13552 encoded a polypeptide comprising 255 amino acid residues. A basic bioinformatics analysis of gsu768 demonstrated a G+C content of 55%. Subsequently, the molecular weight of Gsu768 was estimated to be 28.56 kDa, and the pI value was calculated at 5.88 using the ExPASy Compute pI/Mw algorithm.

Gsu768 has been indicated to show low sequence homology with reported esterase from *Geobacillus* sp.[38–42]. Homology analysis showed that Gsu768 has the highest consistency of 25.91% with esterases from the thermal denitrifying soil bacterium (*Paracoccus denitrificans* Axe2) (Table S2), indicating its high research value. Sequence alignment indicated that Asp201 (D), His237 (H), and Ser116 (S) formed the catalytic triad. The AlphaFold Protein Structure Database was used to predict the 3-D structures of Gsu768, and the 3-D structure of Gsu768 was visualized and modified using PyMOL. The catalytic triad (Asp201 (D), His237 (H), and Ser116 (S)) was observed and was demonstrated in stick form in Fig. 1b. Prediction of the secondary structures showed that the largest proportion (45.49%) of Gsu768 was in the form of an alpha helix, 32.94% as random coil, 14.51% as extended strand, and 7.06% in the form of beta turn. The sequential order and the spatial structure relationship of the secondary structure were shown in the topology diagram (Fig. 1c).

Selection of the Mutation Site and Mutagenesis of Gsu768

The accuracy of a mutation depends on the quality of the model, implying that the protein model quality required evaluation prior to mutation site selection. Two evaluation systems, Verify 3D and PROCHECK were applied. Verify 3D was designed to evaluate the modeling quality using a table computed from the atomic coordinates of a structure employed to score the consistency of the 3D structure model against any amino acid sequence. Based on the above principle, a higher compatibility between the computed structural model and its own sequence results in a higher score. Verify 3D could also examine the profile scores with a moving-window scan to identify incorrectly modeled segments within the correct structure [43]. PROCHECK is a program suite that quickly checks a given structure to highlight any unusual stereochemical profiles and possible errors [44]. Using Verify 3D, a 94.9% score was obtained for the structure, which was significantly higher than the threshold of 80%, and the averaged 3D-1D score was greater than or equal to 0.2. As shown in Fig. S2, PROCHECK was used to determine whether the conformation of the protein was reasonable, and the Ramachandran plot exhibited 204, 16, 0, and 1 residues in the most

favored, additional allowed, generously allowed, and disallowed regions, respectively. Generally, the proportion of the amino acid residues falling in the most favored region and the additional allowed region was higher than 90%, the conformation of the model conformed to the rules of stereochemistry, and the obtained proportion of 99.5% for the predicted model was significantly higher than 90%, indicating excellent quality. After verification using the two evaluation systems, the quality of the Gsu768 protein model was determined sufficient for the subsequent simulated mutagenesis experiments.

As described in the "Materials and Methods" section, the ADAP strategy involves the application of AutoDock, Discovery Studio, and PoPMuSiC, which were applied to determine mutation sites based on their own principles. The binding pocket is considered a significant target when modifying enzyme characteristics, such as substrate specificity or catalytic activity [45]. Therefore, the binding pocket was considered the structure with the best Gibbs free energy (ΔG), which was determined using Auto Dock 4.2.6. Lower ΔG values led to higher stability of the structure [46]. The predicted model with the highest homology was chosen as the acceptable receptor protein, and the C6 molecule obtained from PubChem was used as a ligand. Receptor proteins and ligand molecules were set with charge addition, non-polar hydrogen combination, and appropriate atom type assignment, and the torsion tree center of the ligand molecule was defined. Processed receptor proteins and ligands were then subjected to a docking program. The "Center on Ligands" defined a minimum box in which to accept the default ligand-docking parameters, randomizing the posture of the ligand before docking, and the default parameters in "Genetic Algorithm Parameters" were used, except for the "Number of GA Runs," which was set at 50. The other docking parameters were specified in "Docking Parameters" [47]. The obtained conformations were then sorted according to binding energy, and the conformation with the lowest binding energy was selected for further experiments. The docking results were visualized in Discovery Studio 3.5, and the "Pocket Atoms" are displayed in Fig. S3. To improve the positive mutation rate and obtain more stable mutants, the design principles described in the "Materials and Methods" section were followed. The residues in the binding pocket were displayed and identified using Discovery Studio 3.5, which was then used to calculate the mutation energy for saturation mutation of the binding pocket residues. As shown in Fig. S3, 19 residues (F36, F46, L76, Q78, W82, S116, M117, G119, I120, L138, M139, S145, A146, D201, Q202, V203, P205, H237, and V239) were selected, and the simulated mutagenesis results were exhibited after the mutation energy was calculated using Discovery Studio 3.5 (Table S3). The results of saturation mutation resulted in the mutation energy for 361 mutants, of which 71 showed better stability, 75 demonstrated no significant change, and 215 displayed instability. Based on the first selection criterion, the 71 most stable mutants were recognized as positive mutations and chosen for further study. Nineteen residues in the binding pocket were then mutated and analyzed in three modules of PoPMuSiC to determine their $\Delta\Delta G$, ΔTm, and thermal stability. PoPMuSiC allows any changes in the stability resulting from all possible point mutations in an average-sized protein to be estimated in a few seconds [48] The process was introduced by Gilis and Rooman [49] to estimate the folding free energy changes between WT and variants using linear combinations of database-derived potentials, and it was a useful tool for computer-aided rational mutation design [50]. However, because of the limitations of certain computational algorithms, the rational design approach could be challenging. Algorithm optimization [51, 52] designing novel approaches, and the integration of various methods [53] have been commonly employed to enhance the positive rate. Thus, two methods (PoPMuSiC and Discovery Studio 3.5), which were based on different calculation principles, were used to screen the mutation sites.

As shown in Tables S4, S5, and S6, 3 mutation results were obtained that included 58 mutants with $\Delta\Delta G < 0$, 40 with $\Delta Tm > 0$, and 17 with thermal stability +. Based on the selection criteria, the results of the mutation simulation are listed in Table S7, in which the mutation sites that were selected and further investigated (Q78F, Q78I, Q78Y, G119A, G119C, and S145W) were listed in bold.

Expression, Purification, and Enzymatic Properties of Gsu768 and Its Mutants

Gsu768 was inserted into the pET-28a (+) vector for expression in *E. coli*. The predicted molecular mass of 28.56 kDa that was obtained for the recombinant Gsu768 was consistent with that estimated by SDS-PAGE (Fig. S4). The primers that were used to construct the mutants are listed in Table S8. Mutants were constructed in the pET-28a (+) vector using the same method and expressed in *E. coli*. Protein expression was verified by SDS-PAGE (Fig. S5).

After obtaining six mutants, their enzymatic activity and thermal stability were determined on a preliminary basis. As shown in Fig. 2, most mutants showed increased enzyme activity, whereas Q78F showed a significant decrease. The thermostability of Q78I, Q78Y, and G119A, which retained 28%, 87%, and 27% of their residual activity after incubation at 70 °C for 20 min, respectively, were improved in comparison with the 19% residual activity observed for WT, where the thermostability of Q78I, Q78Y, and G119A was increased by 47%, 357%, and 42%, respectively. The thermostability of other single-point mutants (Q78F, G119C, and S145W) was not remarkably enhanced; therefore, they were not

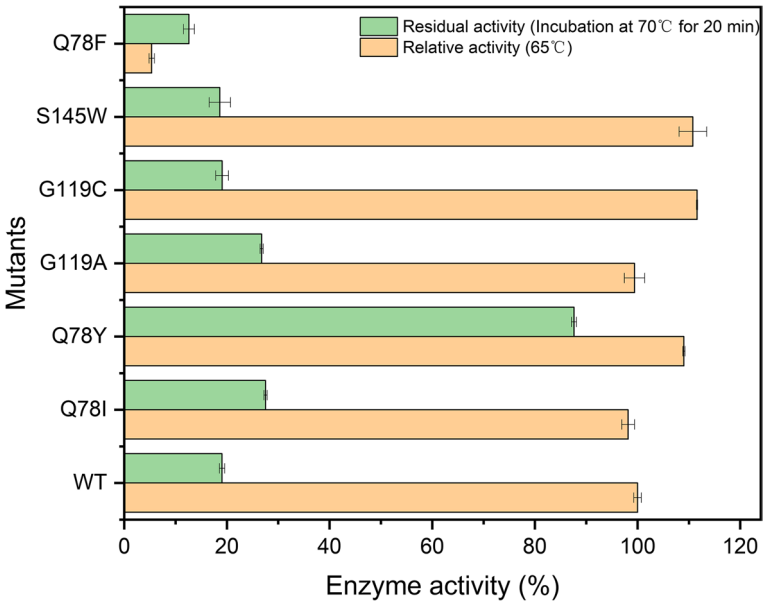

Fig. 2 The relative enzyme activities and thermal stability of WT and single-point mutants. Orange box: the relative enzyme activities of WT and single-point mutants. In these experiments, the enzyme activity of WT under standard assay conditions (65 °C) was defined as 100%. Green box: thermal stability at 70 °C (incubation for 20 min) of WT and single-point mutants. The relative enzyme activity of the enzyme before incubation was defined as 100%. All experiments were performed at least in triplicates

considered for subsequent investigations. To further enhance the enzyme characteristics, a double-point mutant (Q78Y/G119A) was constructed to explore the synergistic effect of the two single-point mutants with improved properties. Subsequently, the characteristics of mutants Q78I, Q78Y, G119A, and Q78Y/G119A were investigated.

To identify the substrate specificity of the mutants, the relative activities against both short-chain substrates and long-chain substrates (C2–C16) of the three single-point mutants and the double-point mutant were determined and compared with those of the WT. As shown in Fig. 3a, short-chain nitrobenzenes were the preference substrate which was consistent with that of the WT, especially C6, and the mutants had a certain hydrolytic ability for long-chain nitrobenzenes. Compared with that in the WT, the enzyme activities of mutants for substrates with longer chains were inferior to those with shorter chains, indicating that chain-length selectivity had shifted to short chains. The hydrolytic ability of the four mutants improved for C2 and C16, whereas it decreased slightly for the other substrates, especially the double-point mutant, which demonstrated that the synergistic effect of several positive single-point mutations was not necessarily better than that of the single-point mutation in terms of substrate specificity. In addition, Q78Y showed different substrate preferences and was more inclined to hydrolyze C8 than C6. The optimal substrate of the double-point mutant Q78Y/G119A was C6 instead of the C8 preferred by Q78Y, which was similar to the results reported by Dai et al. [54].

The relative enzyme activity profiles of the WT and its mutants in the temperature range of 55–80 °C and the pH range of 7.0–10.0 were also determined to explore the effects of temperature and pH on enzyme activity (Fig. 3b, c). The results indicated that the optimal temperature increased from 65 to 70 °C for Q78I, Q78Y, and Q78Y/G119A. In addition, Q78I and Q78Y showed lower activity than WT at 55 °C, indicating that two single-point mutants preferred high-temperature reaction conditions. Meanwhile, Q78Y/G119A

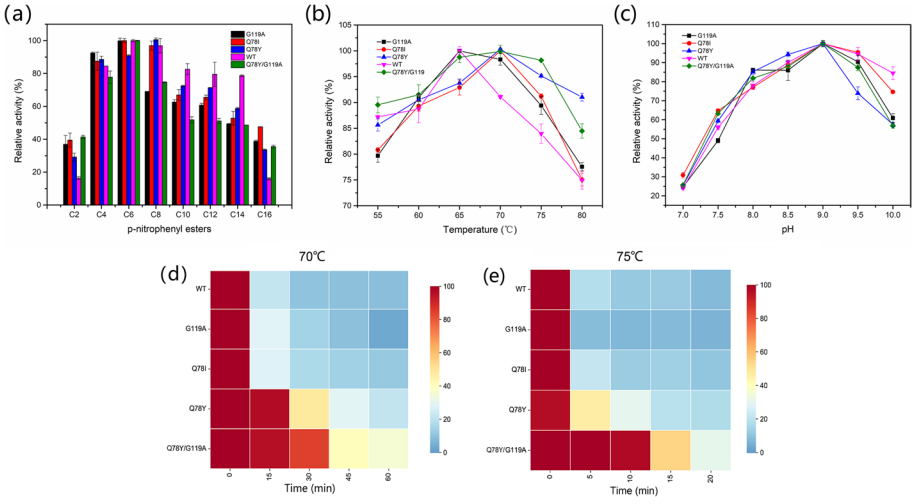

Fig. 3 The relative enzyme activities, enzymatic properties, and the thermal stability at 70 °C and 75 °C of WT and its mutants. **a** Effect of p-nitrophenyl esters of different chain lengths on the activity of WT and its mutants. The effect of **b** temperature and **c** pH on the enzyme activities of the WT and its mutants. The relative enzyme activity of the enzyme under optimal conditions was defined as 100%. At 70 °C **d** and 75 °C **e**, thermal stability of WT and its mutants. X axis was incubation time. The relative enzyme activity of the enzyme before incubation was defined as 100%. All experiments were performed at least in triplicates

retained more than 90% of its maximal enzyme activity over the range of 55–75 °C, whereas WT only maintained higher enzyme activity at the optimal temperature of 65 °C, indicating wider temperature adaptability for the mutant. Little difference was observed between the WT and its mutants in terms of pH, with all mutants preserving more than 70% of their maximal enzyme activities in the pH range from 8.0 to 9.5. The optimal pH of 9.0 indicated that all the obtained mutants were suitable for alkaline reaction conditions.

To investigate thermal stability, the WT and its mutants were incubated at 70 and 75 °C and their residual enzyme activities measured at different times (Fig. 3d, e). Four mutants were able to maintain higher residual activities than WT after 45-min incubation; however, the residual activity of G119A was lower than that of WT following incubation for 60 min. In contrast, Q78Y exhibited superior thermal stability compared with that of the other mutants. Q78Y/G119A, the double-point mutant, exhibited the best thermal stability at 70 °C, retaining 40% of its maximal enzyme activity after 60-min incubation. The $T_{1/2}$ of 42.2 min for Q78Y/G119A at 70 °C was 340% higher than that of WT (9.6 min). In order to further verify the superiority of our protocol, thermal stabilities were also measured at 75 °C. Q78Y showed only 20% activity after incubation at 75 °C for 15 min, which compared to the 98% residual activity observed at 70 °C, indicating a decrease of 78%. The thermal stability of the double-point mutant at 75 °C was greatly improved as compared to both the WT and single-point mutants, with their activity remaining above 50% after incubation for 15 min (Fig. S6). The $T_{1/2}$ of 16.9 min at 75 °C for Q78Y/G119A was 412% higher than that of the WT (3.3 min). Overall, the single-point mutants selected using our protocol achieved significant results, whereas the double-point mutant showed better thermal stability at both 70 °C and 75 °C.

As mentioned above, the optimum temperature of Q78Y/G119A was increased by 5 °C, from 65 to 70 °C, and the thermal stability was significantly improved. Subsequently, PyMOL was used to display and compare the structures of the WT and Q78Y/G119A, which was attended to clarify the mechanism (Fig. S7a). For further elucidation, the mutation energy of Q78Y/G119A was calculated at − 3.56 kcal/mol using Discovery Studio 3.5. Compared with the − 1.57 kcal/mol for Q78Y and − 2.16 kcal/mol for G119A, Q78Y/G119A showed the lowest mutation energy, indicating that it was the most stable of the structures. Intramolecular forces are important factors for free energy and structural stability. Researchers have shown that increasing the intramolecular forces could significantly improve enzyme thermostability [55–57]. Discovery Studio 3.5 was therefore used to analyze the interaction forces between Q78, G119, Y78, and A119 and the surrounding amino acids. As shown in Fig. S7b, c, additional hydrogen bonds were formed by the introduced mutations. The substitution of Q78 with Y78 improved the thermal stability by introducing an additional hydrogen bond, Pi-sulfur, and a Pi-Pi T-shaped structure, enhancing the intramolecular interactions. Simultaneously, A119 formed a new hydrogen bond with T122 and two new alkyl/Pi-alkyl groups with F123 and A137 in the mutant, which were not detected in the WT (Fig. S7d, e). In conclusion, the mechanisms underlying the promotion of enzymatic thermostability appeared to have been the introduction of six additional intramolecular forces in Q78Y/G119A, which may contribute to the decreased flexibility in the local region and enhance thermostability.

Apart from the forces involved in the intramolecular interaction, the B-factor (relative vibrational motion) and root-mean-square fluctuations (RMSFs) were also used to evaluate the structural flexibility. Depending on the flexibility, different regions of a protein can be classified as moderately to highly flexible. The prediction program PredyFlexy (fast computations of only protein sequences) [58] has been reported to provide accurate predictions of structural flexibility without the need for CPU/GPU-intensive calculations [59]. Therefore, PredyFlexy was employed

to evaluate the flexibility of the WT and Q78Y/G119A, which was represented by the B-factor and RMSFs. PredyFlexy classifies protein regions as rigid, intermediate, or flexible structures (Fig. S8). As shown in Table S9, "0," "1," and "2" represent rigid, intermediate, or flexible, respectively. Lowering the B-factor and RMSF values led to highly stable residues, and a higher confidence index led to more accurate predictions. The exchange of glutamine for tyrosine at position 78 led to decreases in both the B-factor and RMSF and an increase in the confidence index, indicating that the mutant became more stable. The amino acid at position 119 showed a similar trend. Researchers have found that more thermodynamically stable proteins frequently exhibit better structural stability [60]. Our results were consistent with these findings. Compared with the WT, Q78Y/G119A showed a lower B-factor and RMSF and higher thermal stability.

In view of the above experimental results, the thermal stability of the double-point mutant was better than that of the single-point mutants; therefore, the subsequent experiments were mainly based on Q78Y/G119A.

The influences of metal ions, chemical reagents, and organic solvents on the activities of the Q78Y/G119A mutant and WT were then investigated. As shown in Table 1, the effects of metal ions (Mn^{2+}, Co^{2+}, Ca^{2+}, Cu^{2+}, Zn^{2+}, Mg^{2+}, and Fe^{2+}) were examined at three different concentrations. The WT strain incubated with 5 mM Ca^{2+} exhibited distinct enzyme activation, while simultaneously showing enzyme inhibition at 1 mM Ca^{2+} and weak promotion at 10 mM Ca^{2+}. In contrast, Q78Y/G119A showed more stable activity at different Ca^{2+} concentrations, with 5 mM Ca^{2+} resulting in only slight modification in terms of enzymatic activity. Pakpimol et al. [61] reported that lipase EQ3 activity was strongly enhanced in the presence of Ca^{2+} (with 124% relative activity). Furthermore, Ca^{2+} has been shown to promote the catalytic activity of esterases from *Pichia lynferdii* Y-7723 [62]. Metal ions could stabilize the optimal activity conformation of an enzyme by combining with the enzyme to activate or strengthen its catalytic activity [63]. However, not all metal ions promoted enzymatic activity. The results showed that Zn^{2+} inhibited the enzyme activity of both the WT and Q78Y/G119A, and the inhibition become more significant as the concentration increased. Lee et al. [64] reported similar results, with Zn^{2+} decreasing the activity of a novel esterase (Est3S) by approximately 90%.

Table 1 Effect of various metal ions on Gsu768 and its mutant activity

Metal-ion compounds	Relative activity (%)[a]					
	WT			Q78Y/G119A		
	1 mM	5 mM	10 mM	1 mM	5 mM	10 mM
Control	100.0	100.0	100.0	100.0	100.0	100.0
Mn^{2+}	82.0 ± 2.8	79.8 ± 0.9	52.7 ± 0.5	81.9 ± 1.3	80.0 ± 1.5	83.4 ± 0.1
Co^{2+}	100.3 ± 1.7	75.3 ± 0.3	47.0 ± 0.7	97.0 ± 0.5	72.3 ± 0.7	22.1 ± 0.5
Ca^{2+}	85.9 ± 2.9	110.7 ± 0.5	101.8 ± 2.6	105.0 ± 2.1	107.4 ± 0.3	102.1 ± 0.6
Cu^{2+}	99.4 ± 0.1	79.9 ± 1.9	31.5 ± 0.4	84.5 ± 0.9	65.9 ± 0.5	34.8 ± 0.3
Zn^{2+}	80.6 ± 0.5	44.4 ± 0.9	34.0 ± 2.9	82.2 ± 0.5	71.6 ± 2.0	43.7 ± 0.6
Mg^{2+}	102.5 ± 0.9	103.2 ± 1.7	96.0 ± 0.6	88.7 ± 0.2	107.0 ± 2.0	101.3 ± 0.8
Fe^{2+}	99.4 ± 1.9	68.4 ± 0.5	53.9 ± 0.8	101.2 ± 2.7	78.6 ± 0.3	55.3 ± 1.2

[a]After incubating WT and Q78Y/G119A for 30 min at room temperature with different concentrations and types of metal ions, the residual enzymatic activity was measured in 50 mM Tris–HCl buffer (pH 9.0) at optimum temperature using C6 as the test substrate. The enzyme sample incubated in buffer only was set as 100%. The presented results were the average of three repeated experiments with SD of ± 5%

Ionic and non-ionic surfactants are widely employed reagents used to investigate esterase properties. For most enzymes, low concentrations of non-ionic surfactants significantly improved the enzyme reaction rate, whereas the charged groups in ionic surfactants disrupted the conformation of the enzyme and thus inhibited enzyme activity. The anionic surfactant SDS and non-ionic surfactants Tween 20, Tween 80, and Triton X-100 were thus selected to determine the effects on WT and Q78Y/G119A enzyme activity. The results in Table 2 showed enhanced enzyme activity with exposure to 1% Tween 20 and Triton X-100 for the WT, and increasing the concentration to 10%, four surfactants were found to inhibit enzyme activity, especially SDS, which inactivated the enzyme.

Generally, esterases and lipases from microorganisms, particularly those of thermophilic microorganisms, have strong resistance to organic solvents. To characterize the organic solvent tolerance of WT and Q78Y/G119A, two polar solvents (ethyl acetate and acetone) and five non-polar solvents (n-hexane, acetonitrile, isooctane, 1,4-dioxane, and trichloromethane) were selected to determine the effect of organic solvents on the activities of WT and Q78Y/G119A (Table 3). Ethyl acetate, n-hexane, and 1,4-dioxane exhibited the same trend as that observed in the WT, enhancing the activity. Subsequent higher concentrations of 1,4-dioxane resulted in higher enzyme activity, with the concentration changing from 50 to 90%, which is a 135.4% increase in activity. However, 90% acetone and acetonitrile had some inhibitory effects on enzyme activity compared to that of 50% acetone. Interestingly, the same organic solvents had different effects on the activities of the WT and Q78Y/G119A. For the Q78Y/G119A, the relative activity increased as the concentrations of ethyl acetate, n-hexane, and isooctane increased, whereas in the presence of acetone, acetonitrile, 1,4-dioxane, and trichloromethane weakened the relative activity. Furthermore, n-hexane significantly strengthened the enzymatic activities of both the WT and Q78Y/G119A, which was particularly interesting and requires further research. Researchers have shown that hexane could reduce the free activation energy of enzymatic reactions and enhance enzyme activities; hexane had positive effects on the catalytic activity of the *Burkholderia cepacian* lipase at both low and high concentrations [65].

Table 2 Effect of various chemical reagents on Gsu768 and its mutant activity

Chemical reagents	Relative activity (%)[a]			
	WT		Q78Y/G119A	
	1%	10%	1%	10%
Control	100.0	100.0	100.0	100.0
Tween 20	107.0 ± 0.1	26.6 ± 0.1	121.3 ± 0.1	34.1 ± 1.3
Tween 80	87.0 ± 2.2	25.4 ± 0.5	118.1 ± 0.6	52.4 ± 0.9
Triton X-100	114.0 ± 0.3	38.5 ± 1.5	117.6 ± 0.1	29.3 ± 1.3
SDS	98.9 ± 0.5	N.D.[b]	98.9 ± 0.2	2.6 ± 0.9

[a]After incubating WT and Q78Y/G119A for 30 min at room temperature in different concentrations and types of chemical reagents, the residual enzymatic activity was measured in 50 mM Tris–HCl buffer (pH 9.0) at optimum temperature using C6 as the test substrate. The enzyme sample incubated in buffer only was set as 100%. The presented results were the average of three repeated experiments with SD of ± 5%; [b]*N.D.* not detectable

Table 3 Effect of various organic solvents on Gsu768 and its mutant activity

Organic solvents	Relative activity (%) [a]			
	WT		Q78Y/G119A	
	50%	90%	50%	90%
Control	100.0	100.0	100.0	100.0
Ethyl acetate	119.3 ± 1.2	180.3 ± 2.1	111.6 ± 0.1	141.3 ± 0.5
Acetone	60.1 ± 1.3	94.9 ± 0.5	93.7 ± 1.6	95.9 ± 0.2
N-hexane	119.1 ± 1.5	105.3 ± 2.0	131.2 ± 1.9	145.7 ± 1.3
Acetonitrile	6.7 ± 2.0	92.6 ± 0.8	4.2 ± 0.3	112.1 ± 0.9
Isooctane	94.1 ± 1.9	87.2 ± 1.1	131.5 ± 1.7	140.6 ± 1.8
1,4-dioxane	166.2 ± 2.3	235.4 ± 2.0	91.4 ± 1.3	96.8 ± 0.4
Trichloromethane	6.4 ± 1.5	1.8 ± 0.2	4.2 ± 0.3	N.D.[b]

[a]After incubating WT and Q78Y/G119A for 1 h at room temperature in different concentrations and types of organic solvents, the residual enzymatic activity was measured in 50 mM Tris–HCl buffer (pH 9.0) at optimum temperature using C6 as the test substrate. The enzyme sample incubated in buffer only was set as 100%. The presented results were the average of three repeated experiments with SD of ± 5%; [b]*N.D.* not detectable

K_m and V_{max} were the core characteristics of an enzyme and were determined using the Michaelis–Menten model in this study. The K_m and V_{max} values of the WT and its mutants were calculated using the Lineweaver–Burk double reciprocal mapping method. At pH 9.0, C6, and the respective optimum temperatures (WT and Q78I: 65 °C, Q78Y, G119A, and Q78Y/G119A: 70 °C), K_m values of 0.53, 0.26, 0.43, 0.43, and 0.31 mM were obtained for the WT, Q78I, Q78Y, G119A, and Q78Y/G119A, respectively (Table 4). A lower K_m indicated stronger binding affinity, and all mutants exhibited lower K_m values than those in WT. Compared to the WT, the affinity of Q78Y/G119A for the substrate increased by 41.51%. Compared to C6, Q78Y displayed a higher affinity for C8, which was consistent with the determination of the enzymatic properties. The specific activities of the purified WT and its mutants are listed in Table 4. Q78Y showed the highest specific activity at 29,786.13 U/mg; however, the specific activity of the double-point mutant Q78Y/G119A decreased slightly, to 28598.92 U/mg.

Table 4 Kinetic parameters of Gsu768 and its mutants on pNP-esters

	Substrate	K_m (mM)	V_{max} (μmol/min)	Specific activity (U/mg)
WT	pNP-hexanoate (C6)	0.53 ± 0.03	55.76 ± 2.50	9804.76
Q78I	pNP-hexanoate (C6)	0.26 ± 0.01	90.84 ± 5.65	14,928.78
Q78Y	pNP-hexanoate (C6)	0.43 ± 0.05	20.43 ± 1.51	29,786.13
G119A	pNP-hexanoate (C6)	0.43 ± 0.02	54.53 ± 3.54	8106.55
Q78Y/G119A	pNP-hexanoate (C6)	0.31 ± 0.03	25.50 ± 1.92	28,598.92
Q78Y	pNP-caprylate (C8)	0.17 ± 0.01	49.93 ± 1.37	29,786.13

Reactions were conducted in pH 9.0 and respective optimum temperature

Synthesis of Cinnamyl Acetate

Cinnamyl acetate, an important edible compound, was explored and employed to expand the application of esterases. In this study, vinyl acetate was selected as the acyl donor to synthesize cinnamyl acetate through transesterification using the WT and Q78Y/G119A whole-cell catalysts (Fig. 4a). Compared with purified enzymes, the significant benefit of synthesizing cinnamyl acetate with whole-cell biocatalysts was the low production cost [25]. Qualitative characterization of cinnamyl acetate was performed using TLC (Fig. 4b), and quantitative analysis using GC (Fig. 4c). In addition to the detection method, the reaction solvent was another important factor in the synthesis of cinnamyl acetate, as the solvent used could affect the conversion and reaction rates by changing the 3-D conformation of the enzyme [66, 67]. In addition, the reaction solvent influences the solubility of the reaction substrate, affecting the binding efficiency. Therefore, the organic solvent was the preliminary factor chosen for investigation as it may affect the conversion rate, and it was selected with different log values. Reactions were performed under the same conditions except for the reaction solvents. As shown in Fig. 5a, the seven solvents had significantly different effects on the transesterification reaction, with the lowest conversion rate observed for 1,4-dioxane and the highest conversion rate for isooctane. Isooctane was thus selected as the optimal organic solvent for subsequent experimentation. To consider total conversion, the conversion rates for different substrate concentrations were explored (Fig. 5b), and to maximize the conversion rate, total conversion amount, and reaction economy, a 0.3 M substrate concentration was employed. Increasing the substrate concentration led to a gradual

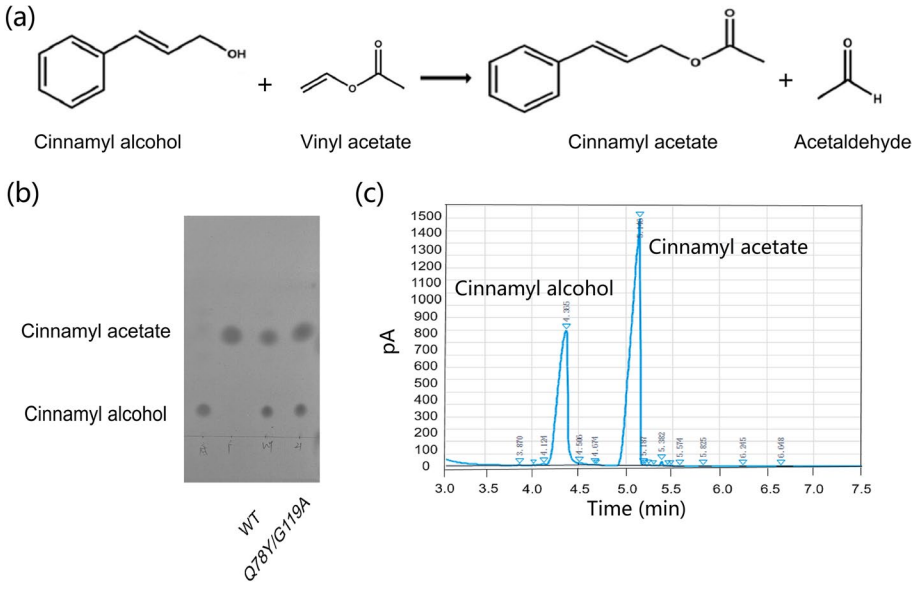

Fig. 4 Synthesis of cinnamyl acetate uses the whole-cell catalyst of WT and Q78Y/G119A. **a** The chemical equation for preparing cinnamyl acetate by transesterification. **b** Thin-layer chromatography (TLC) analysis of the formation of cinnamyl alcohol and cinnamyl acetate. **c** Gas chromatographic analysis of the formation of cinnamyl alcohol and cinnamyl acetate

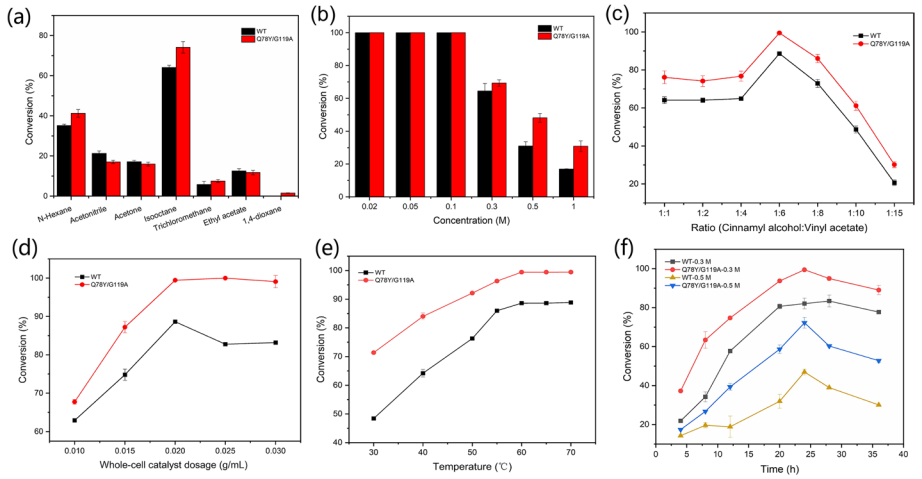

Fig. 5 Optimization of cinnamyl acetate synthesis by the whole-cell catalyst via GC. **a** Effect of solvent on conversion of cinnamyl alcohol. **b** Effect of cinnamyl alcohol concentration on conversion. **c** Effect of substrate molar ratio on the conversion of cinnamyl alcohol. **d** Effect of whole-cell catalysts dosage on the conversion of cinnamyl alcohol. **e** Effect of temperature on conversion of cinnamyl alcohol. **f** Effect of time on conversion of cinnamyl alcohol

decrease in the conversion rate; thus, a substrate concentration of 0.3 M was selected for subsequent experimentation. The effect of the cinnamyl alcohol-to-vinyl acetate molar ratio was also investigated (Fig. 5c). As the substrate molar ratio increased from 1:1 to 1:6, the conversion rate of cinnamyl alcohol was observed to increase; however, this trend gradually decreased after the substrate molar ratio of 1:6, which was therefore selected as the optimum molar ratio. In terms of enzyme dosage, the conversion rate of cinnamyl alcohol increased alongside the whole-cell catalyst increase from 0.01 to 0.03 g/mL; thus, 0.02 g/mL was chosen as the optimal dosage considering the reaction economy (Fig. 5d). Temperature was an important factor that affected the conversion rate, and not only influenced the activity and thermal stability of esterases but also affected the reaction balance and properties of the reaction medium [68, 69]. Considering the characteristics of thermophilic esterase, the conversion rates were studied at 30–70 °C (Fig. 5e), with results showing a gradual increase in the conversion rate with temperature increasing from 30 to 60 °C before the plateau was attained. In view of the boiling point of the solvent, 60 °C was considered to be the optimal reaction temperature at which the highest transesterification activity could be achieved. Thus, the relationship between the reaction duration and conversion rate of cinnamyl alcohol was studied under the optimum conditions (vinyl acetate as the acyl donor, isooctane as the solvent, molar ratio = 1:6, temperature = 60 °C), with results indicating that compared to the WT, Q78Y/G119A showed better catalytic activity at different temperatures and reaction durations (Fig. 5f). At 12 h, the conversion rate of WT reached 57.72%, whereas that of Q78Y/G119A reached 74.72%. At 60 ℃, for Q78Y/G119A, the conversion rate of cinnamyl alcohol was 99.4% after 24 h of reaction, while WT only reached 82.10% under the same conditions. Simultaneously, after optimization under different conditions, the conversion rate of 0.5 M cinnamyl alcohol by WT and Q78Y/G119A was enhanced from 31.04 and 48.18 to 46.95 and 72.24%, respectively. The quantitative analysis results of WT and Q78Y/G119A at 0.3 M and 0.5 M cinnamyl alcohol

concentrations are shown in Fig. S9. In conclusion, the highest conversion rate of 99.4% was achieved after the conditions were optimized with 0.3 M substrate, and the conversion rate of 0.5 M substrate was also enhanced by the optimization.

In contrast to Novozym 435, which was reported to have a conversion rate of only 90.06% under optimal conditions in previous research investigating the synthesis of cinnamyl acetate [23] using cinnamyl alcohol as the substrate and ethyl acetate as the acyl donor, we obtained a higher conversion rate at higher temperatures, lower molar ratios, and lower enzyme loadings. Isooctane was employed as the reaction solvent and lipase TLIM was used as the biological catalyst for the synthesis of cinnamyl acetate, in which, the reaction system was pre-balanced for 3 d to obtain the initial water activity [69]. Nevertheless, our reaction was performed in a non-water system, which can significantly simplify the procedure and reduce the redundancy of time-consuming processes. In addition, PP1113 was employed for the synthesis of cinnamyl acetate, with the highest conversion rate of 94% obtained after optimization [70]. In summary, the developed biocatalyst, when employed for the synthesis of cinnamyl acetate, exhibited a high conversion rate.

Conclusions

In this study, a thermophilic esterase was obtained from wild-type strain *G. subterraneus* DSMZ 13552, and a strategy employing and integrating the rational design tools AutoDock, Discovery Studio, and PoPMuSiC (ADAP) was used to select and design several single-point mutants. Subsequently, a double-point mutant was obtained by combining those single-point mutants with significantly improved thermal stability, which further improved the thermal stability. Furthermore, the enzymatic properties of those mutants were analyzed, demonstrating that Q78Y/G119A was superior, with an enhanced thermostability of 320% as compared to the WT observed under conditions of 70 °C, pH 9, and 15 min. The optimum temperature of the Q78Y/G119A was increased from 65 to 70 °C, indicating that Y78 and A119 were pivotal to the thermostability. Q78Y/G119A was then used in transesterification to synthesize cinnamyl acetate using vinyl acetate and cinnamyl alcohol as substrates. With the 0.3 M substrate, the conversion rate of the cinnamyl acetate synthesis reached 99.4% after optimization of the reaction conditions. In summary, the new thermophilic esterase from *Geobacillus* sp. that was developed through the ADAP strategy in this study showed improved thermal stability, potentially enhancing its application value in the spice industry.

Supplementary Information The online version contains supplementary material available at https://doi.org/10.1007/s12010-023-04697-2.

Author Contribution Jin Zhang: exploration, executing experiments, investigation, software, formal analysis, bioinformatics analysis, data curation, and writing an original draft. Lin Lin: resources and revision. Wei Wei: revision and editing. Dongzhi Wei: revision.

Funding This research was supported by the Shanghai Natural Science Foundation (No. 20ZR1415400), the Shanghai outstanding technical leaders plan 19XD1431900, 19XD1431800, the National Natural Science Foundation of China (Grant No. 81830052, 81530053), and Shanghai Key Laboratory of Molecular Imaging (18DZ2260400).

Data Availability All data generated or analyzed during this study are included in this published article.

Declarations

Ethics Approval Not applicable.

Consent to Participate Not applicable.

Consent for Publication Not applicable.

Competing Interests The authors declare no competing interests.

References

1. Li, M., Lu, Y., & Xu, X. (2022). Mapping the scientific structure and evolution of renewable energy for sustainable development. *Environmental Science and Pollution Research International, 29*, 64832–64845.
2. Shao, H., Xu, L., & Yan, Y. (2013). Isolation and characterization of a thermostable esterase from a metagenomic library. *Journal of Industrial Microbiology and Biotechnology, 40*, 1211–1222.
3. Houde, A., Kademi, A., & Leblanc, D. (2004). Lipases and their industrial applications: An overview. *Applied Biochemistry and Biotechnology, 118*, 155–170.
4. Martínez-Martínez, M., Coscolín, C., Santiago, G., Chow, J., Stogios, P. J., Bargiela, R., Gertler, C., Navarro-Fernández, J., Bollinger, A., Thies, S., Méndez-García, C., Popovic, A., Brown, G., Chernikova, T. N., García-Moyano, A., Bjerga, G. E. K., Pérez-García, P., Hai, T., Del Pozo, M. V., … The Inmare, C. (2018). Determinants and prediction of esterase substrate promiscuity patterns. *ACS Chemical Biology, 13*, 225–234.
5. Li, X. J., Zheng, R. C., Wu, Z. M., Ding, X., & Zheng, Y. G. (2014). Thermophilic esterase from *Thermomyces lanuginosus*: Molecular cloning, functional expression and biochemical characterization. *Protein Expression and Purification, 101*, 1–7.
6. D'Auria, S., Herman, P., Lakowicz, J. R., Tanfani, F., Bertoli, E., Manco, G., & Rossi, M. (2000). The esterase from the thermophilic eubacterium *Bacillus acidocaldarius*: Structural-functional relationship and comparison with the esterase from the hyperthermophilic archaeon *Archaeoglobus fulgidus*. *Proteins, 40*, 473–481.
7. Guo, Y.-Y., Yu, X.-W., & Xu, Y. (2016). Cloning, expression and characterization of two thermostable esterases from *Aquifex aeolicus* VF5. *Journal of Molecular Catalysis B: Enzymatic, 133*, S220–S229.
8. Moore, J. C., Rodriguez-Granillo, A., Crespo, A., Govindarajan, S., Welch, M., Hiraga, K., Lexa, K., Marshall, N., & Truppo, M. D. (2018). "Site and mutation"-specific predictions enable minimal directed evolution libraries. *ACS Synthetic Biology, 7*, 1730–1741.
9. Qiu, J., Yang, H., Shao, Y., Li, L., Sun, S., Wang, L., Tan, Y., & Xin, Z. (2021). Enhancing the activity and thermal stability of a phthalate-degrading hydrolase by random mutagenesis. *Ecotoxicology and Environmental Safety, 209*, 111795.
10. Wehrmann, M., & Klebensberger, J. (2018). Engineering thermal stability and solvent tolerance of the soluble quinoprotein PedE from *Pseudomonas putida* KT2440 with a heterologous whole-cell screening approach. *Microbial Biotechnology, 11*, 399–408.
11. Yu, H., Ma, S., Li, Y., & Dalby, P. A. (2022). Hot spots-making directed evolution easier. *Biotechnology Advances, 56*, 107926.
12. Han, N., Miao, H., Ding, J., Li, J., Mu, Y., Zhou, J., & Huang, Z. (2017). Improving the thermostability of a fungal GH11 xylanase via site-directed mutagenesis guided by sequence and structural analysis. *Biotechnology for Biofuels, 10*, 133.
13. Wang, C., Huang, R., He, B., & Du, Q. (2012). Improving the thermostability of alpha-amylase by combinatorial coevolving-site saturation mutagenesis. *BMC Bioinformatics, 13*, 263.
14. Bonarek, P., Loch, J. I., Tworzydło, M., Cooper, D. R., Milto, K., Wróbel, P., Kurpiewska, K., & Lewiński, K. (2020). Structure-based design approach to rational site-directed mutagenesis of β-lactoglobulin. *Journal of Structural Biology, 210*, 107493.
15. Watanabe, S., Ito, M., & Kigawa, T. (2021). DiRect: Site-directed mutagenesis method for protein engineering by rational design. *Biochemical and Biophysical Research Communications, 551*, 107–113.

16. da Silva, F. B., de Oliviera, V. M., Sanches, M. N., Contessoto, V. G., & Leite, V. B. P. (2020). Rational design of chymotrypsin inhibitor 2 by optimizing non-native interactions. *Journal of Chemical Information and Modeling, 60*, 982–988.
17. Eason, M. G., Damry, A. M., & Chica, R. A. (2017). Structure-guided rational design of red fluorescent proteins: Towards designer genetically-encoded fluorophores. *Current Opinion in Structural Biology, 45*, 91–99.
18. Porro, A., Binda, A., Pisoni, M., Donadoni, C., Rivolta, I., & Saponaro, A. (2020). Rational design of a mutation to investigate the role of the brain protein TRIP8b in limiting the cAMP response of HCN channels in neurons. *Journal of General Physiology, 152*, e202012596.
19. Inamoto, I., Sheoran, I., Popa, S. C., Hussain, M., & Shin, J. A. (2021). Combining rational design and continuous evolution on minimalist proteins that target the E-box DNA site. *ACS Chemical Biology, 16*, 35–44.
20. Pan, H., Kong, S., Fu, X., Li, X., & Guo, D. (2020). De novo biosynthesis of cinnamyl acetate in engineered *Escherichia coli*. *Biochemical Engineering Journal, 164*, 107796.
21. Schrader, J., Etschmann, M. M., Sell, D., Hilmer, J. M., & Rabenhorst, J. (2004). Applied biocatalysis for the synthesis of natural flavour compounds–current industrial processes and future prospects. *Biotechnology Letters, 26*, 463–472.
22. Li, B., Li, Y., Bai, D., Zhang, X., Yang, H., Wang, J., Liu, G., Yue, J., Ling, Y., Zhou, D., & Chen, H. (2014). Whole-cell biotransformation systems for reduction of prochiral carbonyl compounds to chiral alcohol in *Escherichia coli*. *Science and Reports, 4*, 6750.
23. Geng, B., Wang, M., Qi, W., Su, R., & He, Z. (2012). Cinnamyl acetate synthesis by lipase-catalyzed transesterification in a solvent-free system. *Biotechnology and Applied Biochemistry, 59*, 270–275.
24. Wu, Z., Qi, W., Wang, M., Su, R., & He, Z. (2014). Lipase immobilized on novel ceramic supporter with Ni activation for efficient cinnamyl acetate synthesis. *Journal of Molecular Catalysis B: Enzymatic, 110*, 32–38.
25. Dong, H., Secundo, F., Xue, C., & Mao, X. (2017). Whole-cell biocatalytic synthesis of cinnamyl acetate with a novel esterase from the DNA library of *Acinetobacter hemolyticus*. *Journal of Agriculture and Food Chemistry, 65*, 2120–2128.
26. Thompson, J. D., Higgins, D. G., & Gibson, T. J. (1994). CLUSTAL W: Improving the sensitivity of progressive multiple sequence alignment through sequence weighting, position-specific gap penalties and weight matrix choice. *Nucleic Acids Research, 22*, 4673–4680.
27. Gouet, P., Courcelle, E., Stuart, D. I., & Métoz, F. (1999). ESPript: Analysis of multiple sequence alignments in PostScript. *Bioinformatics, 15*, 305–308.
28. Wilkins, M. R., Gasteiger, E., Bairoch, A., Sanchez, J. C., Williams, K. L., Appel, R. D., & Hochstrasser, D. F. (1999). Protein identification and analysis tools in the ExPASy server. *Methods in Molecular Biology, 112*, 531–552.
29. Jumper, J., Evans, R., Pritzel, A., Green, T., Figurnov, M., Ronneberger, O., Tunyasuvunakool, K., Bates, R., Žídek, A., Potapenko, A., Bridgland, A., Meyer, C., Kohl, S. A. A., Ballard, A. J., Cowie, A., Romera-Paredes, B., Nikolov, S., Jain, R., Adler, J., … Hassabis, D. (2021). Highly accurate protein structure prediction with AlphaFold. *Nature, 596*, 583–589.
30. Varadi, M., Anyango, S., Deshpande, M., Nair, S., Natassia, C., Yordanova, G., Yuan, D., Stroe, O., Wood, G., Laydon, A., Žídek, A., Green, T., Tunyasuvunakool, K., Petersen, S., Jumper, J., Clancy, E., Green, R., Vora, A., Lutfi, M., … Velankar, S. (2022). AlphaFold Protein Structure Database: Massively expanding the structural coverage of protein-sequence space with high-accuracy models. *Nucleic Acids Research, 50*, D439-d444.
31. Laskowski, R. A., MacArthur, M. W., Moss, D. S., & Thornton, J. M. (1993). PROCHECK: A program to check the stereochemical quality of protein structures. *Journal of Applied Crystallography, 26*, 283–291.
32. Lüthy, R., Bowie, J. U., & Eisenberg, D. (1992). Assessment of protein models with three-dimensional profiles. *Nature, 356*, 83–85.
33. Bowie, J. U., Lüthy, R., & Eisenberg, D. (1991). A method to identify protein sequences that fold into a known three-dimensional structure. *Science, 253*, 164–170.
34. Morris, G. M., Huey, R., Lindstrom, W., Sanner, M. F., Belew, R. K., Goodsell, D. S., & Olson, A. J. (2009). AutoDock4 and AutoDockTools4: Automated docking with selective receptor flexibility. *Journal of Computational Chemistry, 30*, 2785–2791.
35. Dehouck, Y., Grosfils, A., Folch, B., Gilis, D., Bogaerts, P., & Rooman, M. (2009). Fast and accurate predictions of protein stability changes upon mutations using statistical potentials and neural networks: PoPMuSiC-2.0. *Bioinformatics, 25*, 2537–2543.
36. Cai, X., Lin, L., Shen, Y., Wei, W., & Wei, D. Z. (2020). Functional expression of a novel methanol-stable esterase from *Geobacillus subterraneus* DSM13552 for biocatalytic synthesis of cinnamyl acetate in a solvent-free system. *BMC Biotechnology, 20*, 36.

37. Gao, W., Wu, K., Chen, L., Fan, H., Zhao, Z., Gao, B., Wang, H., & Wei, D. (2016). A novel esterase from a marine mud metagenomic library for biocatalytic synthesis of short-chain flavor esters. *Microbial Cell Factories, 15*, 41.
38. Ewis, H. E., Abdelal, A. T., & Lu, C. D. (2004). Molecular cloning and characterization of two thermostable carboxyl esterases from *Geobacillus stearothermophilus*. *Gene, 329*, 187–195.
39. Bravman, T., Zolotnitsky, G., Shulami, S., Belakhov, V., Solomon, D., Baasov, T., Shoham, G., & Shoham, Y. (2001). Stereochemistry of family 52 glycosyl hydrolases: A beta-xylosidase from *Bacillus stearothermophilus* T-6 is a retaining enzyme. *FEBS Letters, 495*, 39–43.
40. Mølgaard, A., Kauppinen, S., & Larsen, S. (2000). Rhamnogalacturonan acetylesterase elucidates the structure and function of a new family of hydrolases. *Structure, 8*, 373–383.
41. Daas, M. J. A., Nijsse, B., van de Weijer, A. H. P., Groenendaal, B., Janssen, F., van der Oost, J., & van Kranenburg, R. (2018). Engineering *Geobacillus thermodenitrificans* to introduce cellulolytic activity; expression of native and heterologous cellulase genes. *BMC Biotechnology, 18*, 42.
42. Ay Sal, F., Colak, D. N., Guler, H. I., Canakci, S., & Belduz, A. O. (2019). Biochemical characterization of a novel thermostable feruloyl esterase from *Geobacillus thermoglucosidasius* DSM 2542(T). *Molecular Biology Reports, 46*, 4385–4395.
43. Eisenberg, D., Lüthy, R., & Bowie, J. U. (1997). VERIFY3D: Assessment of protein models with three-dimensional profiles. *Methods in Enzymology, 277*, 396–404.
44. Morris, A. L., MacArthur, M. W., Hutchinson, E. G., & Thornton, J. M. (1992). Stereochemical quality of protein structure coordinates. *Proteins, 12*, 345–364.
45. Bornscheuer, U. T. (2002). Microbial carboxyl esterases: Classification, properties and application in biocatalysis. *FEMS Microbiology Reviews, 26*, 73–81.
46. Aisyafalah, S., Hudiyanti, D., Asy'ari, M., & Siahaan, P. (2021). Probing the interaction of HAV4 peptide (Ac-SHAVAS-NH 2) with E-cadherin domain EC1-EC2 by molecular docking. *Journal of Physics: Conference Series, 1943*, 012163.
47. Forli, S., Huey, R., Pique, M. E., Sanner, M. F., Goodsell, D. S., & Olson, A. J. (2016). Computational protein-ligand docking and virtual drug screening with the AutoDock suite. *Nature Protocols, 11*, 905–919.
48 Dehouck, Y., Kwasigroch, J. M., Gilis, D., & Rooman, M. (2011). PoPMuSiC 2.1: A web server for the estimation of protein stability changes upon mutation and sequence optimality. *BMC Bioinformatics, 12*, 151.
49. Gilis, D., & Rooman, M. (2000). PoPMuSiC, an algorithm for predicting protein mutant stability changes: Application to prion proteins. *Protein Engineering, 13*, 849–856.
50. Zhang, S. B., & Wu, Z. L. (2011). Identification of amino acid residues responsible for increased thermostability of feruloyl esterase A from *Aspergillus niger* using the PoPMuSiC algorithm. *Bioresource Technology, 102*, 2093–2096.
51. Traoré, S., Roberts, K. E., Allouche, D., Donald, B. R., André, I., Schiex, T., & Barbe, S. (2016). Fast search algorithms for computational protein design. *Journal of Computational Chemistry, 37*, 1048–1058.
52. Kuhlman, B., & Bradley, P. (2019). Advances in protein structure prediction and design. *Nature Reviews Molecular Cell Biology, 20*, 681–697.
53. Chen, T. S., & Keating, A. E. (2012). Designing specific protein-protein interactions using computation, experimental library screening, or integrated methods. *Protein Science, 21*, 949–963.
54 Komiya, D., Hori, A., Ishida, T., Igarashi, K., Samejima, M., Koseki, T., & Fushinobu, S. (2017). Crystal structure and substrate specificity modification of acetyl xylan esterase from *Aspergillus luchuensis*. *Applied and Environment Microbiology, 83*, e01251.
55. Ruslan, R., Rahman, R., Leow, T. C., Ali, M. S. M., Basri, M., & Salleh, A. B. (2012). Improvement of thermal stability via outer-loop ion pair interaction of mutated T1 lipase from *Geobacillus zalihae* strain T1. *International Journal of Molecular Sciences, 13*, 943–960.
56. Yu, Z., Yu, H., Xu, J., Wang, Z., Wang, Z., Kang, T., Chen, K., Pu, Z., Wu, J., Yang, L., & Xu, G. (2022). Enhancing thermostability of lipase from *Pseudomonas alcaligenes* for producing l-menthol by the CREATE strategy. *Catalysis Science & Technology, 12*, 2531–2541.
57. Zhu, Y., Qiao, C., Li, H., Li, L., Xiao, A., Ni, H., & Jiang, Z. (2018). Improvement thermostability of *Pseudoalteromonas carrageenovora* arylsulfatase by rational design. *International Journal of Biological Macromolecules, 108*, 953–959.
58. de Brevern, A. G., Bornot, A., Craveur, P., Etchebest, C., & Gelly, J. C. (2012). PredyFlexy: Flexibility and local structure prediction from sequence. *Nucleic Acids Research, 40*, W317-322.
59. Gyulkhandanyan, A., Rezaie, A. R., Roumenina, L., Lagarde, N., Fremeaux-Bacchi, V., Miteva, M. A., & Villoutreix, B. O. (2020). Analysis of protein missense alterations by combining sequence- and structure-based methods. *Molecular Genetics & Genomic Medicine, 8*, e1166.
60. Nutschel, C., Coscolín, C., David, B., Mulnaes, D., Ferrer, M., Jaeger, K. E., & Gohlke, H. (2021). Promiscuous esterases counterintuitively are less flexible than specific ones. *Journal of Chemical Information and Modeling, 61*, 2383–2395.

61. Ungcharoenwiwat, P., & H-Kittikun, A. (2015). Purification and characterization of lipase from *Burkholderia* sp. EQ3 isolated from wastewater from a canned fish factory and its application for the synthesis of wax esters. *Journal of Molecular Catalysis B: Enzymatic, 115*, 96–104.
62. Kim, H. R., Kim, I. H., Hou, C. T., Kwon, K. I., & Shin, B. S. (2010). Production of a novel cold-active lipase from *Pichia lynferdii* Y-7723. *Journal of Agriculture and Food Chemistry, 58*, 1322–1326.
63. Chang, H. C., Chen, L. Y., Lu, Y. H., Li, M. Y., Chen, Y. H., Lin, C. H., & Chang, G. G. (2007). Metal ions stabilize a dimeric molten globule state between the open and closed forms of malic enzyme. *Biophysical Journal, 93*, 3977–3988.
64. Lee, H. Y., Cho, D. Y., Ahmad, I., Patel, H. M., Kim, M. J., Jung, J. G., Jeong, E. H., Haque, M. A., & Cho, K. M. (2021). Mining of a novel esterase (est3S) gene from a cow rumen metagenomic library with organosphosphorus insecticides degrading capability: Catalytic insights by site directed mutations, docking, and molecular dynamic simulations. *International Journal of Biological Macromolecules, 190*, 441–455.
65. Mohtashami, M., Fooladi, J., Haddad-Mashadrizeh, A., Housaindokht, M. R., & Monhemi, H. (2019). Molecular mechanism of enzyme tolerance against organic solvents: Insights from molecular dynamics simulation. *International Journal of Biological Macromolecules, 122*, 914–923.
66. Duarte, S. H., Hernández, G. L., Canet, A., Benaiges, M. D., Maugeri, F., & Valero, F. (2015). Enzymatic biodiesel synthesis from yeast oil using immobilized recombinant *Rhizopus oryzae* lipase. *Bioresource Technology, 183*, 175–180.
67. Nasaruddin, R. R., Alam, M. Z., & Jami, M. S. (2014). Evaluation of solvent system for the enzymatic synthesis of ethanol-based biodiesel from sludge palm oil (SPO). *Bioresource Technology, 154*, 155–161.
68. Yadav, G. D., & Devendran, S. (2012). Lipase catalyzed synthesis of cinnamyl acetate via transesterification in non-aqueous medium. *Process Biochemistry, 47*, 496–502.
69. Wang, Y., Zhang, D. H., Zhang, J. Y., Chen, N., & Zhi, G. Y. (2016). High-yield synthesis of bioactive ethyl cinnamate by enzymatic esterification of cinnamic acid. *Food Chemistry, 190*, 629–633.
70. Tang, X.-D., Dong, F.-Y., Zhang, Q.-H., Lin, L., Wang, P., Xu, X.-Y., Wei, W., & Wei, D.-Z. (2021). Protein engineering of a cold-adapted rhamnogalacturonan acetylesterase: In vivo functional expression and cinnamyl acetate synthesis. *Process Biochemistry, 107*, 129–137.

Authors and Affiliations

Jin Zhang[1] · Lin Lin[2,3] · Wei Wei[1] · Dongzhi Wei[1]

✉ Wei Wei
weiwei@ecust.edu.cn

Jin Zhang
2837767740@qq.com

Lin Lin
linlin21023@163.com

Dongzhi Wei
dzhwei@ecust.edu.cn

[1] State Key Laboratory of Bioreactor Engineering, Newworld Institute of Biotechnology, East China University of Science and Technology, Shanghai 200237, People's Republic of China

[2] School of Chemical and Environmental Engineering, Shanghai Institute of Technology, Shanghai 201418, People's Republic of China

[3] Research Laboratory for Functional Nanomaterial, National Engineering Research Center for Nanotechnology, Shanghai 200241, People's Republic of China